Check for updates

Molecular Microbiology

WILEY

RESEARCH ARTICLE

Pseudomonas aeruginosa Relies on a Phosphoketolase to Support Anaerobic Survival Under Reductive Stress

Richard D. Horak[1] | Nanqing Zhou[2] | Korbinian O. Thalhammer[3] | Nathan F. Dalleska[4] | Ludmilla Aristilde[2,5] | Dianne K. Newman[1,3]

[1]Division of Biology and Biological Engineering, California Institute of Technology, Pasadena, California, USA | [2]Department of Civil and Environmental Engineering, McCormick School of Engineering and Applied Science, Northwestern University, Evanston, Illinois, USA | [3]Division of Geological and Planetary Sciences, California Institute of Technology, Pasadena, California, USA | [4]Water and Environment Laboratory, California Institute of Technology, Pasadena, California, USA | [5]Northwestern Center for Synthetic Biology, Northwestern University, Evanston, Illinois, USA

Correspondence: Dianne K. Newman (dkn@caltech.edu)

Received: 20 December 2025 | **Revised:** 12 February 2026 | **Accepted:** 16 February 2026

ABSTRACT

Across diverse contexts, bacteria experience loss of electron acceptors due to fluctuating environmental conditions, leading to growth-arrest and reductive stress. Yet, microbial metabolism has been primarily studied with cells growing under nutrient-replete conditions. To study how cells preserve metabolic flux under reductively stressed growth-arrest, we explored how the opportunistic pathogen *Pseudomonas aeruginosa* remodels its metabolism under such conditions. During anaerobic survival on glucose, *P. aeruginosa* utilizes the upper Embden-Meyerhoff-Parnas pathway and pentose-phosphate pathway to generate metabolite precursors for a previously undescribed phosphoketolase (herein termed *xfp*) used to produce acetyl-P and indirectly ATP via subsequent acetate formation. This re-routing bypasses *P. aeruginosa*'s canonical glucose-catabolizing Entner-Doudoroff pathway (EDP), allowing for metabolic flux without exacerbating reductive stress. Moreover, anaerobic survival on diverse carbon sources triggers purine degradation and metabolite accumulation, requiring *xfp* to maintain metabolic balance and viability. Thus, our data suggest that phosphoketolases may play an additional role in ribonucleotide balance. This study expands our understanding of *P. aeruginosa*'s anaerobic survival strategies and serves as a reminder that large gaps remain in our understanding of growth arrest physiology even in well-studied model organisms, highlighting the potential for basic discovery in the realm of non-growth metabolism.

1 | Introduction

Despite the immense diversity of metabolic strategies across the tree of life, the rules underpinning them are remarkably unified. All life must couple energy generation with energy expenditures (e.g., biosynthesis); a process accomplished via carefully managed redox reactions (Chubukov et al. 2014). Loss of redox balance, such as an inability to consume excess reducing equivalents (i.e., reductive stress), leads to metabolic disruption, growth arrest, and even cellular death (Xiao and Loscalzo 2020). From the perspective of human biology, reductive stress is commonly thought to be purely detrimental due to its linkage to a variety of illnesses (Cantó et al. 2015; Luo et al. 2024; Ying 2008; Yang et al. 2025). Yet, microorganisms are commonly found in oxidant-limited environments, such as in bioreactors, soil communities, and human infections (Silver et al. 1999; Enfors et al. 2001; Cowley et al. 2015; Voroney and Heck 2015; Bergkessel et al. 2016). While numerous studies have uncovered diverse fermentative metabolisms to support growth under reductive stress (Bartacek et al. 2007; Hackmann and Zhang 2023; Hackmann 2024; Thauer et al. 1977), we know far less about the metabolic strategies supporting growth-arrested survival in bacteria reliant on respiration for growth.

Within the metabolism field, a historic focus on bacterial growth has led to many organisms being defined as "non-fermentative" or

© 2026 John Wiley & Sons Ltd.

"obligate aerobes" based on their inability to grow under oxidant-limited conditions. Yet many of these bacteria contain fermentation genes. For example, in the traditionally deemed "obligate aerobe" *Mycobacterium smegmatis*, cells can utilize fermentative hydrogen production to alleviate reductive stress and generate ATP during hypoxia-induced growth arrest (Berney et al. 2014). A related phenomenon is observed in human biology, with hypoxia and mitochondrial dysfunction stimulating the Warburg effect, whereby glycolysis outpaces respiration, leading to lactate production to consume excess reducing equivalents while maintaining ATP production (Warburg 1925; Kukurugya et al. 2024). Because bacteria that rely on aerobic respiration for growth can be challenged by oxygen limitation (Ciemniecki and Newman 2020; Silver et al. 1999; Voroney and Heck 2015), it is likely that these fermentative strategies to support non-growth survival in respiratory organisms may be more common than has been realized.

An alternative to consuming reducing equivalents to maintain metabolic flux under reductive stress is to use metabolic pathways that do not generate reducing equivalents. To test this idea, we turned to the "non-fermentative" pathogen *Pseudomonas aeruginosa*, known to survive for weeks in oxidant-limited growth-arrested states, herein termed "anaerobic survival" (Eschbach et al. 2004). *P. aeruginosa* depends on respiration of molecular oxygen or via denitrification to support exponential growth (Gayon and Dupetit 1886; Zumft 1997); it is unable to grow exponentially in the absence of terminal electron acceptors. However, it can metabolize arginine and yeast extract for slight anaerobic growth or ferment pyruvate to support anaerobic survival (Vander Wauven et al. 1984). In the case of the latter, pyruvate is metabolized to acetate via acetyl-CoA and acetyl-phosphate (acetyl-P) by the *ackA-pta* system, generating ATP and NADH. Meanwhile, generation of lactate from additional pyruvate molecules via *ldhA* regenerates NAD+ (Eschbach et al. 2004) (Figure 1A).

On carbon sources such as glucose, *P. aeruginosa* also relies on *ackA-pta* for ATP generation and can persist in a non-growth state (Ciemniecki et al. 2024; Glasser et al. 2014). However, glucose-surviving cells can only survive if they employ phenazines—self-made electron shuttles—to alleviate reductive stress (Ciemniecki et al. 2024; Glasser et al. 2014). *P. aeruginosa* lacks a complete upper Embden-Meyerhoff-Parnas pathway (EMPP) for standard glycolysis and lacks the oxidative pentose-phosphate pathway (PPP) (Kohlstedt and Wittmann 2019; Lessie and Phibbs 1984). During aerobic growth, almost all glucose catabolic flux occurs first via oxidation of glucose to gluconate, followed by further oxidation or its phosphorylation, eventually generating 6-phosphogluconate that feeds into the Entner-Doudoroff pathway (EDP) and lower EMPP (Kohlstedt and Wittmann 2019). However, during anaerobic survival this glycolytic pathway would generate excess reducing equivalents ([2e$^-$]) via reduced ubiquinone from initial glucose oxidation and NADPH or NADH from the lower EMPP (Figure 1A). Therefore, we predicted that under reductive stress *P. aeruginosa*'s glucose catabolic flux would shift towards the non-oxidative upper EMPP and PPP by way of glucose-6-phosphate (glucose-6P) and fructose-6-phosphate (fructose-6P).

Precedent for such metabolic re-routing in *P. aeruginosa* exists in the literature. Despite catabolizing glucose to gluconate during aerobic growth (generating reduced ubiquinone), during anaerobic growth on nitrate as a terminal electron acceptor, *P. aeruginosa* instead catabolized all measurable glucose to glucose-6P (Lessie and Phibbs 1984). However, use of the lower EMPP to connect the PPP to acetate and ATP production would still generate excess reducing equivalents, unless paired with lactate production, limiting ATP and acetate yields (Figure 1A). An alternative non-oxidative path connecting the PPP to acetate production is via phosphoketolases, one such protein being previously discovered and purified from *P. aeruginosa* ATCC 15442 (Petrareanu et al. 2014).

Phosphoketolases are thiamine-pyrophosphate-dependent enzymes that catalyze the phosphorolysis of fructose-6-phosphate (fructose-6P), xylulose-5-phosphate (xylulose-5P), and/or sedoheptulose-7-phosphate (sedoheptulose-7P), releasing 2 carbons from each substrate as acetyl-P and generating erythrose-4-phosphate (erythrose-4P), glyceraldehyde-3-phosphate (glyceraldehyde-3P), or ribose-5-phosphate (ribose-5P), respectively (Krüsemann et al. 2018; Sánchez et al. 2010; Suzuki et al. 2010). The activity and preference for each substrate differs across phosphoketolase homologs in different species. Phosphoketolases have been primarily studied for their role in natural product generation and in fermentative metabolisms such as hexose catabolism via the phosphoketolase pathway in some *Lactobacillus* species and the bifido-shunt in *Bifidobacterium* species, as well as pentose catabolism in *Clostridium acetobutylicum* (Aristilde et al. 2015; Årsköld et al. 2008; de Vries and Stouthamer 1967; Liu et al. 2012). Within *C. acetobutylicum*, phosphoketolases provide efficient non-oxidative pentose catabolism while supporting ATP generation. This metabolism bypasses pentose flux through the PPP or EMPP, avoiding rate-limiting enzymatic steps, carbon loss, and generation of additional reducing equivalents (Aristilde et al. 2015; Liu et al. 2012; Servinsky et al. 2012). During energy-limited anaerobic survival in *P. aeruginosa*, a similar strategy would allow for continued ATP production while minimizing protein cost and reducing equivalent generation (Figure 1A). While *P. aeruginosa* contains many of the genes involved in the bifido-shunt, it is unable to consume excess reducing equivalents via ethanol generation through the enzyme ethanol dehydrogenase.

Intriguingly, the phosphoketolase gene of *P. aeruginosa* is regulated by the anaerobic transcription factor Anr and its regulatory small RNA *esrA*, indicating a potential role for phosphoketolases during anaerobic carbon metabolism in this organism (Ferrara et al. 2021; Hammond et al. 2015; Tribelli et al. 2019). Accordingly, we set out to test the hypothesis that during anaerobic survival on glucose, metabolic flux diverts into the non-oxidative PPP, enabling Xfp to utilize PPP metabolites, such as xylulose-5P, to form acetyl-P, ultimately leading to acetate and ATP production while avoiding additional production of reducing equivalents (Figure 1A).

2 | Results

2.1 | *P. aeruginosa* Relies on a Phosphoketolase During Anaerobic Survival on Glucose Under Reductive Stress

Evidence in support of our hypothesis, that during anaerobic survival *P. aeruginosa* catabolizes glucose via the non-oxidative PPP and a putative phosphoketolase, came from

13652958, 2026, 5, Downloaded from https://onlinelibrary.wiley.com/doi/10.1111/mmi.70059 by Claremont Colleges Libraries, Wiley Online Library on [17/11/2026]. See the Terms and Conditions (https://onlinelibrary.wiley.com/terms-and-conditions) on Wiley Online Library for rules of use; OA articles are governed by the applicable Creative Commons License

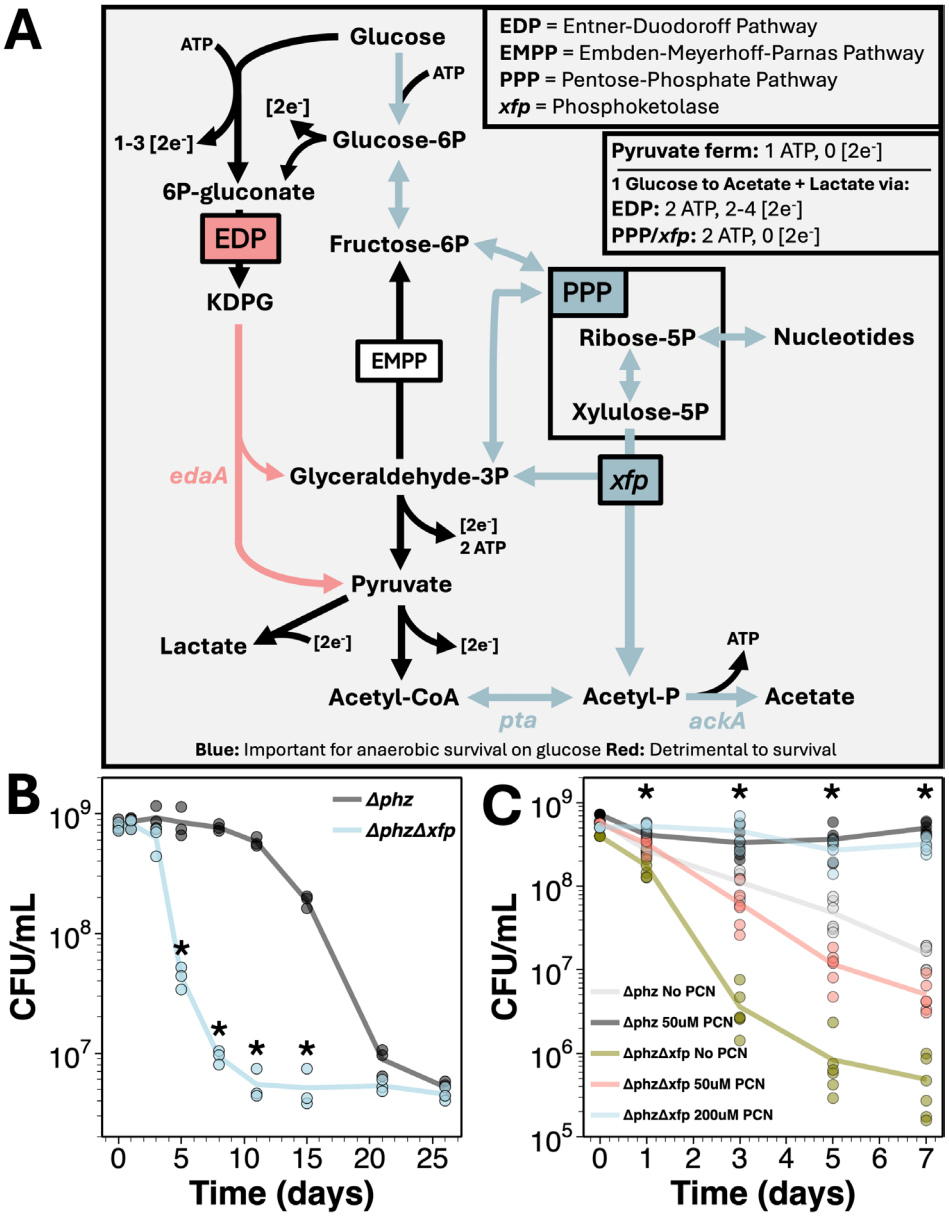


FIGURE 1 | Mutation of PA14's *xfp* diminishes anaerobic survival on glucose but can be rescued by alleviation of reductive stress. (A) Condensed metabolic diagram highlighting the evidence behind our hypothesis that under reductive stress, glucose catabolic flux to acetate would be more favorable by way of the PPP than via the EDP. Blue arrows are pathways or genes that were important for anaerobic survival on glucose while red genes were detrimental (Saunders 2020). All reducing equivalents are written as [2e⁻] for simplicity. KDPG = 2-keto-3-deoxy-6-phosphogluconate. (B) Mutation of *xfp* leads to a drop in anaerobic survival after 3 days in anoxic Balch tubes. Blue = *Δphz*. Grey = *ΔphzΔxfp*. (C) Addition of the electron shuttle phenazine-1-carboxamide (PCN) to increase reducing equivalent consumption rescues survival of the *xfp* mutant during anaerobic survival in a 96-well potentiostat system. Light grey = *Δphz* with no PCN, black = *Δphz* + 50 μM PCN, olive = *ΔphzΔxfp* with no PCN, light red = *ΔphzΔxfp* + 50 μM PCN, light blue = *ΔphzΔxfp* + 200 μM PCN. (B, C) Log transformed CFU per mL values. Carbon source is 20 mM glucose. Starting $OD_{500nm} = 0.75$. Dots are biological replicates, lines represent means. (B) $n = 3$ per condition. (C) $n = 3$–6 per condition. (B) * denotes p value < 0.05 from independent two-tailed t-test comparing each strain for each say. (C) * denotes p value < 0.05 from one-way ANOVA comparing all groups per day.

a preliminary transposon-sequencing (Tn-seq) screen performed in our lab using *P. aeruginosa* UCBPP-PA14 (PA14) surviving anaerobically on glucose in the presence of phenazine-1-carboxylic acid (Saunders 2020). Despite PA14 relying on the EDP for aerobic glucose catabolism, transposon insertions in the core EDP gene *edaA*, catalyzing the formation of glyceraldehyde-3P and pyruvate, or in the positive EDP regulator *hexR*, increased survival on glucose (Figure 1A) (Saunders 2020). Meanwhile, transposon insertion in genes involved in the upper EMPP, the PPP gene transaldolase, the *ackA-pta* system, or a putative phosphoketolase (*PA14_17580*, herein referred to as *xfp*), were all detrimental to PA14's survival (Figure 1A) (Saunders 2020). While PA14's Xfp has not been purified and confirmed for phosphoketolase activity, its amino acid sequence is nearly identical to the previously purified phosphoketolase of *P. aeruginosa* strain ATCC 15442, with

13652958, 2026, 5, Downloaded from https://onlinelibrary.wiley.com/doi/10.1111/mmi.70059 by Claremont Colleges Libraries, Wiley Online Library on [17/11/2026]. See the Terms and Conditions (https://onlinelibrary.wiley.com/terms-and-conditions) on Wiley Online Library for rules of use; OA articles are governed by the applicable Creative Commons License

only two amino acid identities differing (Figure S1). The Xfp of 15,442 was confirmed to have in vitro enzymatic activity on both fructose-6P and xylulose-5P, with a strong preference for the latter (Petrareanu et al. 2014). Therefore, we reasoned that PA14's Xfp might retain this catalytic capability, preferentially consuming xylulose-5P to generate glyceraldehyde-3P and acetyl-P, bridging the non-oxidative PPP and acetate generation to support anaerobic survival and ATP production on glucose.

To determine whether the loss of *xfp* results in a survival deficit during reductively stressed anaerobic survival on glucose, we generated a clean deletion of *PA14_17580*. All experiments were performed in a phenazine-null mutant background (*Δphz*) to avoid alleviation of reductive stress by phenazines and better isolate a Xfp-dependent reductive stress survival mechanism. To test for survival, anoxic cell suspensions of *Δphz* and *ΔphzΔxfp* strains were sampled and plated for colony-forming units (CFUs) over time. Both strains maintained ~100% survival for the first 3 days of anaerobic survival, yet by day 5, *ΔphzΔxfp* CFUs dropped over 2 orders of magnitude before plateauing between 10 and 15 days (Figure 1B). Meanwhile the parent strain *Δphz* maintained ~100% survival for 10 days before losing viability, plateauing to a similar level as the *xfp* mutant—2 orders of magnitude lower than starting CFUs (Figure 1B). Complementation of *xfp* in the *ΔphzΔxfp* strain fully restored viability (Figure S2A). Additionally, there was no effect of the *xfp* mutation during anaerobic growth on glucose using KNO_3 as a terminal electron acceptor (Figure S2B). Finally, to confirm this effect was not due to the *Δphz* background, we additionally generated a *Δxfp* strain in the WT PA14 background, observing no statistical difference between it and the *ΔphzΔxfp* strain (Figure S2A).

To test our assumption that Xfp is only needed under conditions of reductive stress, we repeated the experiment above in a 96-well plate equipped with electrodes, allowing us to determine if the addition of phenazines could rescue the *ΔphzΔxfp* strain. Cells were given 200 μM, 50 μM, or 0 μM of phenazine-1-carboximide (PCN), an endogenous electron shuttle produced by PA14. Each well of the 96-well plate contained a working, reference, and counter electrode, enabling any PCN that is reduced by cells to be reoxidized at the working electrode, allowing for dissipation of reducing equivalents. In support of our hypothesis that reductive stress causes the need for Xfp to maintain viability, we see that 200 μM of PCN rescues the survival of the *ΔphzΔxfp* strain (Figure 1C). Notably, the *Δphz* strain is unable to maintain 100% survival in the absence of PCN, yet 50 μM is enough to promote full viability. However, the *ΔphzΔxfp* strain still dies in the presence of 50 μM PCN, suggesting a greater demand for an electron acceptor to restore redox balance in the *xfp* mutant (Figure 1C). Together, these data suggest that Xfp and phenazines play complementary roles in allowing cells to maintain survival under reductive stress.

2.2 | *P. aeruginosa* Utilizes a Phosphoketolase-Mediated Pathway for Catabolism of Glucose to Acetate During Anaerobic Survival

To verify that PA14 can use its Xfp for glucose catabolism and acetate production, we performed pathway-diagnostic isotopic labelling experiments. Both *Δphz* and *ΔphzΔxfp* strains were incubated with 1-$^{13}C_1$-glucose and supernatants were removed on days 3/5/7 for the *Δphz* strain and on day 3 for *ΔphzΔxfp*. We then measured the relative abundance of acetate and the fraction that was ^{13}C labelled. PA14 relies on *ackA*-mediated ATP generation during anaerobic survival on glucose. Accordingly, if all 1-$^{13}C_1$-glucose is catabolized via the EDP and lower EMPP to form pyruvate and then acetate via *ackA-pta*, we expected all acetate would lack ^{13}C labelling due to loss of ^{13}C as CO_2 during formation of acetyl-CoA (Figure 2A). However, if 1-$^{13}C_1$-glucose were instead catabolized via a bifido-shunt-like phosphoketolase-mediated metabolism, we predicted a fraction of the acetate would be ^{13}C labelled, specifically at the first carbon atom. As PA14 lacks the oxidative PPP, this latter possibility would require glucose to enter the PPP by way of glucose-6P and fructose-6P, where ^{13}C labelled fructose-6P is either directly processed by Xfp, or interconverted to xylulose-5P and/or sedoheptulose-7P, potential Xfp substrates. Cleavage of any of these three potential substrates by Xfp would thus be expected to release singly ^{13}C-labelled acetyl-P, which can then form acetate via *ackA* or acetyl-CoA via *pta*, all of which would be ^{13}C labelled in the first position (Figure 2A). However, the strong homology of PA14's Xfp to a previously purified *P. aeruginosa* phosphoketolase (Petrareanu et al. 2014, Figure S1) suggests a preference for xylulose-5P as a substrate, generating glyceraldehyde-3P and acetyl-P as products, denoted by red boxes in Figure 2A.

By day 3 of anaerobic survival, we observed no significant ^{13}C labelling of acetate from *ΔphzΔxfp* supernatants; meanwhile, ~20% of acetate from *Δphz* samples was singly ^{13}C labelled, increasing to ~40% by day 7 (Figure 2B). Additionally, by day 3, *Δphz* supernatants contained around twice the acetate of *ΔphzΔxfp* supernatants (Figure 2C). While acetate was primarily visible as the acetic acid molecular ion (CH_3COOH^+), in-source fragmentation also allowed detection of the second carbon atom in the form of carboxylic acid cations (HCO_2^+). Despite high levels of singly labelled acetate in *Δphz* supernatants, we were unable to detect substantial doubly ^{13}C labelled acetic acid or singly ^{13}C labelled carboxylic acid fragments. Taken together, these results indicate that acetate produced by *Δphz* cells from 1-$^{13}C_1$-glucose is singly ^{13}C labelled at the methyl position. It is important to note that the fraction of ^{13}C labelled-acetate likely underestimates the contribution of Xfp to acetate generation, as Xfp substrates can also be generated from unlabeled endogenous carbon stores or unlabeled glucose-derived fructose-6P or glyceraldehyde-3P. Regardless, these findings demonstrate that during anaerobic survival on glucose, PA14 can utilize an alternative glucose catabolic pathway for acetate production.

2.3 | *P. aeruginosa* Relies on Xfp for Metabolic Homeostasis of Endogenous Metabolites During Anaerobic Survival on Glucose

Having established that PA14 can utilize a PPP and Xfp-mediated metabolism for acetate generation during anaerobic survival on glucose, we were curious whether Xfp played any additional roles in metabolic homeostasis. To test this, we repeated our anaerobic survival experiments, using the *Δphz* and *ΔphzΔxfp* strains, as well as a *ΔphzΔackAΔpta* strain—unable to generate acetate

13652958, 2026, 5, Downloaded from https://onlinelibrary.wiley.com/doi/10.1111/mmi.70059 by Claremont Colleges Libraries, Wiley Online Library on [17/11/2026]. See the Terms and Conditions (https://onlinelibrary.wiley.com/terms-and-conditions) on Wiley Online Library for rules of use; OA articles are governed by the applicable Creative Commons License

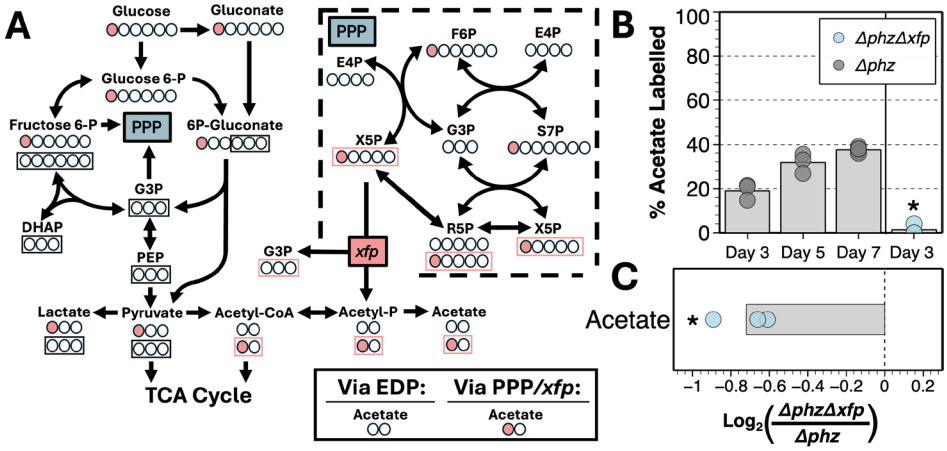


FIGURE 2 | PA14 can utilize the PPP and its phosphoketolase to catabolize glucose to acetate. (A) Abridged central carbon metabolism diagram of PA14 showing initial incorporation/assimilation of 1-$^{13}C_1$-glucose to acetate either via the EDP (glucose ➔ 6P-gluconate ➔ G3P + pyruvate) and lower EMPP (G3P ➔ pyruvate ➔ acetate) or via the PPP (glucose ➔ glucose 6-P ➔ fructose 6-P ➔ X5P) and Xfp activity (X5P ➔ G3P + acetyl-P ➔ acetate). Acetate via the EDP and lower EMPP would be unlabeled while acetate via the PPP and Xfp could be labelled in the first position. Red dots represent ^{13}C label. Black boxes = carbon from the 4,5,6 C atoms of 6P-gluconate. Red boxes = carbon from X5P.(B) Percent of ^{13}C labelled acetate in the parent strain and *xfp* mutant during of anaerobic survival on 20 mM 1-$^{13}C_1$-glucose. (C) Relative abundance of acetate in the *xfp* mutant by day 3 of anaerobic survival on 20 mM glucose, normalized to the parent strain. (B,C) Points show individual biological replicates, $n = 3$. Grey = *Δphz*, blue = *ΔphzΔxfp*. (B) Bars show means of each group. (C) Bar shows mean of *ΔphzΔxfp* metabolite intensities normalized to the mean of *Δphz* levels. (A) PPP = pentose-phosphate pathway. DHAP = dihydroxyacetone phosphate. G3P = glyceraldehyde-3-phosphate. PEP = phosphoenolpyruvate. E4P = erythrose-4-phosphate. F6P = fructose-6-phosphate. X5P = xylulose-5-phosphate. R5P = ribose-5-phosphate. S7P = sedoheptulose-7-phosphate.

or acetyl-CoA from acetyl-P—and a *ΔphzΔackAΔptaΔxfp* strain. Loss of *ackA-pta* is less detrimental than loss of *xfp*, and loss of all three genes is as detrimental as loss of *xfp* alone (Figure 3A). This suggests that both acetate and acetyl-CoA generation from Xfp-derived acetyl-P is dispensable early in survival, implying that Xfp plays an additional role under these conditions.

To identify this role, we repeated our 1-$^{13}C_1$-glucose experiment with the *Δphz* and *ΔphzΔxfp* strains, extracting intracellular metabolites and measuring their relative abundance and fraction of ^{13}C isotopic incorporation. On day 3, 60%–80% of glucose-6P, fructose-6P, and sedoheptulose-7P were ^{13}C labelled in the *Δphz* strain, consistent with flux of glucose into the upper EMPP and PPP. However, in the *ΔphzΔxfp* strain we observed only 20%–40% ^{13}C incorporation for these same metabolites (Figure 3B). Despite lower ^{13}C labelling in *ΔphzΔxfp* cells, upper EMPP and PPP metabolites were ~4–8 times higher than in *Δphz* cells (Figure 3C). The simultaneous low ^{13}C labelling of PPP metabolites and ~4–8 times increase in their abundance in *ΔphzΔxfp* cells suggests input into the PPP, from glucose or endogenous carbon stores, outpaces PPP metabolite consumption. Additionally, as the increase in metabolite abundance is larger than the decrease in ^{13}C labelling for metabolites such as sedoheptulose-7P, these results may suggest that ^{13}C incorporation and PPP influx is faster in *ΔphzΔxfp* cells than *Δphz* cells for some metabolites.

As ^{13}C labelling of upper EMPP and PPP metabolites continued to increase by a few percent in the *Δphz* strain across the 7 days (Figure S3A,B), we noted a decrease in the relative abundance of these metabolites by half (Figure S3C). The presence of doubly and triply ^{13}C labelled ribose-5P and sedoheptulose-7P in *Δphz* cells throughout survival suggests substantial cycling of glucose-derived metabolites through the PPP (Figure 2B, Figure S3B). The lack of detection of acetyl-CoA, absence of significant ^{13}C labelling of TCA cycle metabolites, and lack of detection of ^{13}C labelling of N-acetyl-glutamate, despite its significant consumption in *Δphz* cells throughout survival, leaves us unable to determine if any Xfp-derived acetyl-P is used to form acetyl-CoA (Figure S3A,C,D). Meanwhile, a lack of pyruvate ^{13}C labelling, despite little change in its abundance over 7 days in *Δphz* cells, suggests little flux out of the EDP (Figure 2B). However, EDP metabolites were undetectable, so we cannot comment on levels of flux into the EDP.

To determine which metabolite differences were caused by anaerobic survival or *xfp* loss per se, we compared metabolite abundance in cells before and after the start of our survival experiment. Before anaerobic survival, the *ΔphzΔxfp* strain showed no dramatic differences in PPP metabolites compared to the *Δphz* strain, and though we observed some differences between the strains, such as a 1.5-log decrease in phenylalanine levels in *ΔphzΔxfp* cells, these differences were largely abolished after 3 days of anaerobic survival on glucose (Figure S4A,B). Both strains individually showed an increase of up to 5-fold of upper EMPP, PPP, and TCA cycle metabolites during anaerobic survival compared to their levels beforehand, likely due to lower carbon utilization rates during growth arrest (Figure 3D,E, Figure S4C,D). These results indicate that anaerobic survival itself causes widespread central carbon metabolite accumulation, but that Xfp is important for balancing metabolite influx and consumption, specifically in the upper EMPP and PPP.

2.4 | *P. aeruginosa*'s Xfp Maintains Metabolic Homeostasis and Viability During Anaerobic Survival on Diverse Carbon Sources and in the Absence of Exogenous Carbon

The accumulation of unlabeled EMPP and PPP metabolites in *ΔphzΔxfp* cells from presumptive metabolism of endogenous carbon stores suggested that the *ΔphzΔxfp* strain might

13652958, 2026, 5, Downloaded from https://onlinelibrary.wiley.com/doi/10.1111/mmi.70059 by Claremont Colleges Libraries, Wiley Online Library on [17/11/2026]. See the Terms and Conditions (https://onlinelibrary.wiley.com/terms-and-conditions) on Wiley Online Library for rules of use; OA articles are governed by the applicable Creative Commons License

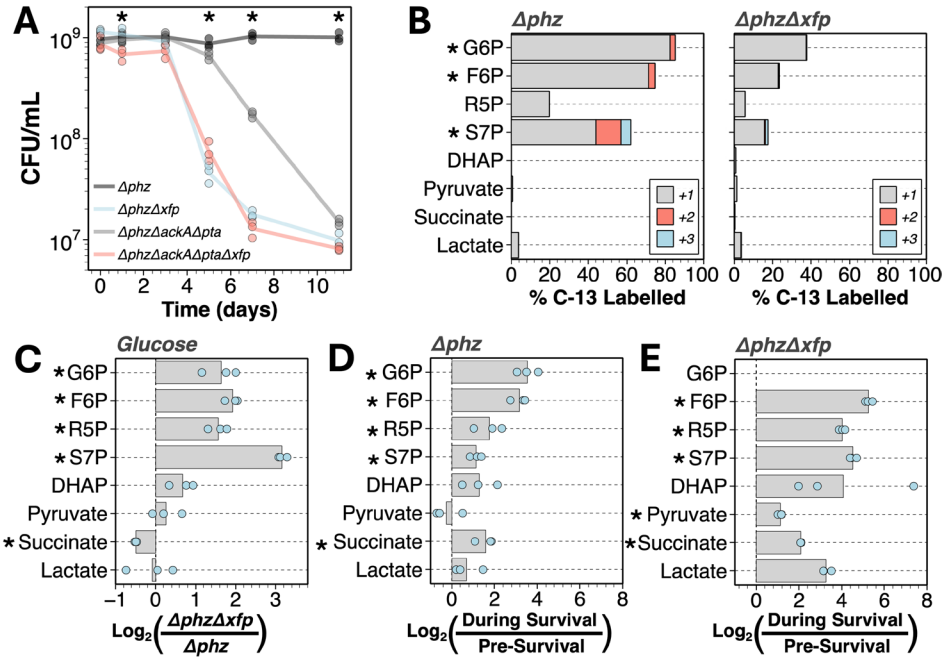


FIGURE 3 | Xfp plays a role in metabolic homeostasis and consumption of endogenous metabolites to support catabolic flux from glucose. (A) Log-transformed CFU/mL values showing loss of the acetate generating system *ackA-pta* does not increase the survival deficit caused by *xfp* mutation. Lines = means, dots = replicates, $n = 3$. * denotes $p < 0.05$ from one-way ANOVA comparing means across all groups per day. (B) Percent of isotopically labelled metabolites in the parent strain and *xfp* mutant. Bars = mean of 3 biological replicates. Grey = singly labelled. Red = doubly labelled. Blue = triply labelled. (C) Log_2 transformed *ΔphzΔxfp* metabolite intensities normalized to the mean of *Δphz* metabolite intensities. Bars = means of *ΔphzΔxfp* normalized intensities, dots = replicates, $n = 3$. (D, E). Log_2 transformed metabolite intensities from *Δphz* samples (D) or *ΔphzΔxfp* samples (E) after 3 days of survival normalized to mean metabolite levels of the same strain before survival, bars = means, dots = independent replicates, $n = 3$. (B–E) * denotes p value < 0.05 from an independent two-tailed t-test comparing means between strains (B, C) or between pre- and post-survival metabolite levels within strains (D, E). G6P = glucose-6-phosphate. F6P = fructose-6-phosphate. R5P = ribose-5-phosphate, which is in equilibrium with xylulose-5-phosphate. S7P = sedoheptulose-7-phosphate. DHAP = dihydroxyacetone phosphate, which is in equilibrium with glyceraldehyde-3-phosphate.

exhibit similar phenotypes when provided with carbon sources other than glucose. Accordingly, we repeated our survival experiments on a variety of carbon sources or the absence of an exogenous carbon source. By Day 7 of anaerobic survival the *ΔphzΔxfp* mutant showed over 10-fold lower CFUs on all carbon sources except for pyruvate, as well as in the no carbon condition (Figure 4A). Additionally, by day 3, we observed mean metabolite levels of upper EMPP and PPP ~2–16 times higher in the *ΔphzΔxfp* strain during survival on succinate, glutamate and in the absence of exogenous carbon, but not on pyruvate (Figure 4B). Differences in some conditions between strains were nonsignificant due to variation in individual replicate metabolite values (Figure S5A). Each carbon source had unique differences between strains (Figure S5A). Metabolite measurements were not made during survival on glycerol, fructose, or butyrate.

Compared to their individual metabolite levels before anaerobic survival, both strains showed general increases in EMPP, PPP, and TCA cycle metabolites in all conditions including pyruvate, likely due to lower carbon utilization during growth arrest (Figure S6A,B). These data further support that metabolite accumulation is a general phenotype of transitioning from aerobic growth to anaerobic survival, but that, as survival continues, Xfp prevents further accumulation of upper EMPP and PPP metabolites. Notably, while trends in metabolite differences between the two strains were the same across all conditions except pyruvate, the magnitude of these changes was different for each nutrient condition (Figure S7). Therefore, different carbon sources likely cause varying levels of carbon influx into the PPP and its related pathways, leading to unique metabolic pressure, potentially explaining the variable importance of Xfp on promoting survival (Figure 4A).

2.5 | Anaerobic Survival Triggers Purine Degradation and Xfp Is Essential for Maintaining Ribonucleotide Homeostasis

Because several studies have observed widespread RNA degradation during nutrient starved growth arrest in diverse bacteria (Deutscher 2003; Himeoka et al. 2022), we hypothesized that release of ribose-5-phosphate during ribonucleotide degradation might explain the accumulation of unlabeled metabolites in the PPP. This notion was bolstered by the fact that studies in mitochondria have shown increased PPP flux and accumulation of ribonucleotides after induction of reductive stress (Wu et al. 2024; Yang et al. 2022, 2025). Moreover, directly upstream of PA14's *xfp* genes are two hypothetical proteins—*PA14_17550* and *PA14_17570*—with homology to LOG-family proteins and MBL-fold metallo-hydrolases with potential RNA and ribonucleotide degradative functions respectively (Baier and Tokuriki 2014; Dzurová et al. 2015; Seo et al. 2016).

13652958, 2026, 5, Downloaded from https://onlinelibrary.wiley.com/doi/10.1111/mmi.70059 by Claremont Colleges Libraries, Wiley Online Library on [17/11/2026]. See the Terms and Conditions (https://onlinelibrary.wiley.com/terms-and-conditions) on Wiley Online Library for rules of use; OA articles are governed by the applicable Creative Commons License

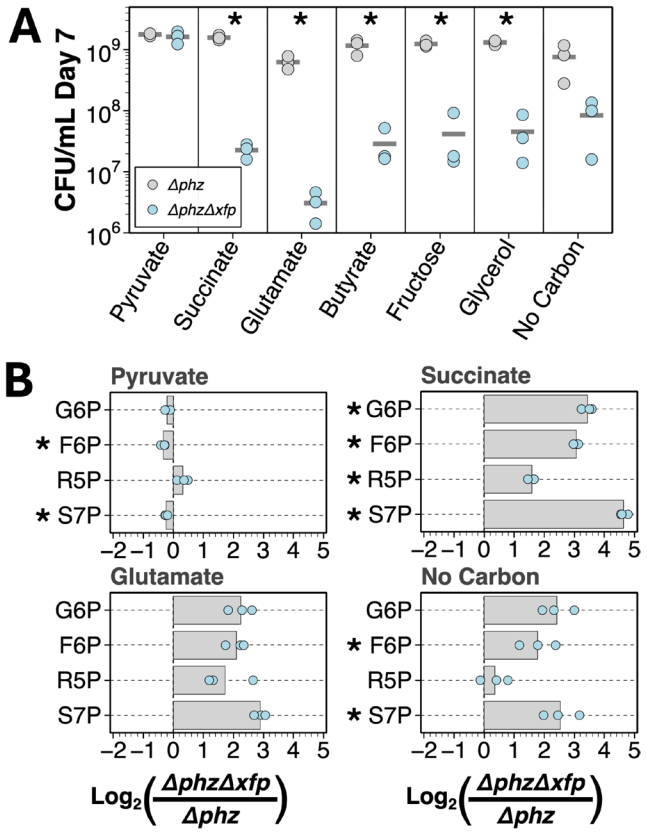


FIGURE 4 | Xfp is important for viability and PPP metabolite homeostasis during anaerobic survival on various carbon sources, but not pyruvate. (A) CFU/mL of the *xfp* mutant and parent strain after 7 days of anaerobic survival on different carbon sources or in the absence of an exogenous carbon source. Grey = *Δphz*, blue = *ΔphzΔxfp*. (B) Log_2 transformed *ΔphzΔxfp* metabolite intensities normalized to the mean *Δphz* metabolite intensities after 3 days of survival on specified carbon sources. (A, B) Bar/dash = mean, dots = independent replicates, $n = 3$. (A, B) * denotes p value < 0.05 from an independent two-tailed t-test comparing the means of each strain per metabolite per condition. G6P = glucose-6-phosphate. F6P = fructose-6-phosphate. R5P = ribose-5-phosphate. S7P = sedoheptulose-7-phosphate. All carbon sources were at a final concentration for 120 mM of total carbon (ex. 20 mM fructose, 40 mM pyruvate, etc.)

To test this hypothesis, we measured xanthine—a purine nucleobase degradation product—before and after anaerobic survival under various conditions. After 3 days of anaerobic survival, xanthine levels were ~4 to 32 times higher in both the *Δphz* and *ΔphzΔxfp* strains across all conditions compared to their pre-survival levels (Figure 5A). Before and during survival, both strains show similar xanthine levels relative to each other, albeit with slight elevation in the *ΔphzΔxfp* strain generally (Figure 5A, Figure S8A). Therefore, this data suggests that, irrespective of Xfp activity, anaerobic survival may trigger purine ribonucleotide degradation and xanthine accumulation, in addition to promoting flux into the PPP via ribose-5P. Alternatively, lowered xanthine consumption (via inhibition of ribonucleotide salvage or xanthine degradation to uric acid) could explain these results.

We further hypothesized that buildup of PPP metabolites in the *ΔphzΔxfp* strain during survival would potentially dysregulate ribonucleotide levels by inhibiting further ribose-5P release during ribonucleotide degradation. After 3 days of anaerobic survival on glucose, ribonucleotides levels were over 4 times higher in the *ΔphzΔxfp* strain compared to *Δphz* cells, except for ATP and dUMP (Figure 5B). Ribonucleotide levels were similarly elevated in *ΔphzΔxfp* cells after 3 days of survival in the absence of an exogenous carbon source, on glutamate, or on succinate compared to *Δphz* cells (Figure 5C, Figure S8B). However, loss of *xfp* did not change ribonucleotide levels during survival on pyruvate (Figure 5C, Figure S8B), similar to its lack of effect on the accumulation of upper PPP metabolites (Figure 4B). Notably, while trends were similar across conditions, metabolite levels and the effect of *xfp* mutation occurred at different magnitudes for different nutrient conditions (Figure S9). This observed increase in ribonucleotide levels in *ΔphzΔxfp* cells compared to *Δphz*, cells despite both strains having similar xanthine levels, may suggest faster ribonucleotide polymer (e.g., RNA) breakdown in *ΔphzΔxfp* cells to form ribonucleotide monomers, but an inhibition of further degradation; alternatively, it may point to increased ribonucleotide biosynthesis. Follow-up studies are needed to distinguish between these possibilities. Regardless, our data suggest that Xfp plays a role in ribonucleotide homeostasis.

To determine if, as seen with PPP and upper EMPP metabolite levels, ribonucleotide accumulation generally occurred upon transition to anaerobic survival, irrespective of *xfp*, we compared the metabolite levels of each strain during survival to their own levels before survival began. Compared to before survival, ribonucleotide levels only generally increased by 2 times or more in *Δphz* cells during survival on glucose, but not on other substrates, compared to *Δphz* cells before survival began (Figure S10A,B). In contrast, ribonucleotide levels were generally ~2–64 times higher in *ΔphzΔxfp* cells during survival on all substrates except pyruvate compared to *ΔphzΔxfp* cells before survival began (Figure S10C). Both strains individually showed lower ATP levels during survival compared to before on all substrates except for pyruvate and showed large increases upwards of 64 times higher in dUMP levels during survival on pyruvate (Figure S10B,C). Therefore, while xanthine accumulation and loss of ATP occur during anaerobic survival irrespective of *xfp*, ribonucleotide accumulation is generally specific to *ΔphzΔxfp* cells. As ribonucleotide accumulation is only correlated with PPP metabolite accumulation in *ΔphzΔxfp* cells, this suggests a role for Xfp in mediating ribonucleotide degradation and/or recycling.

Overall, our data reveal that anaerobic survival triggers purine degradation and PPP metabolite accumulation, necessitating Xfp to maintain homeostasis of these metabolite pools during survival on non-pyruvate carbon sources. We hypothesize that Xfp is necessary because consumption of accumulated PPP metabolites by other pathways would be inhibited under reductive stress, such as the EDP or lower EMPP, or require substantial energetic costs, such as ribonucleotide biosynthesis (Figure 5D). Meanwhile, during survival on pyruvate, compared to survival in other nutrient conditions, a relatively higher adenylate charge and/or lower reductive stress conditions could make non-Xfp pathways for metabolite consumption viable, abolishing a need for Xfp activity to maintain metabolic balance. Finally, the increase in AMP and

13652958, 2026, 5, Downloaded from https://onlinelibrary.wiley.com/doi/10.1111/mmi.70059 by Claremont Colleges Libraries, Wiley Online Library on [17/11/2026]. See the Terms and Conditions (https://onlinelibrary.wiley.com/terms-and-conditions) on Wiley Online Library for rules of use; OA articles are governed by the applicable Creative Commons License

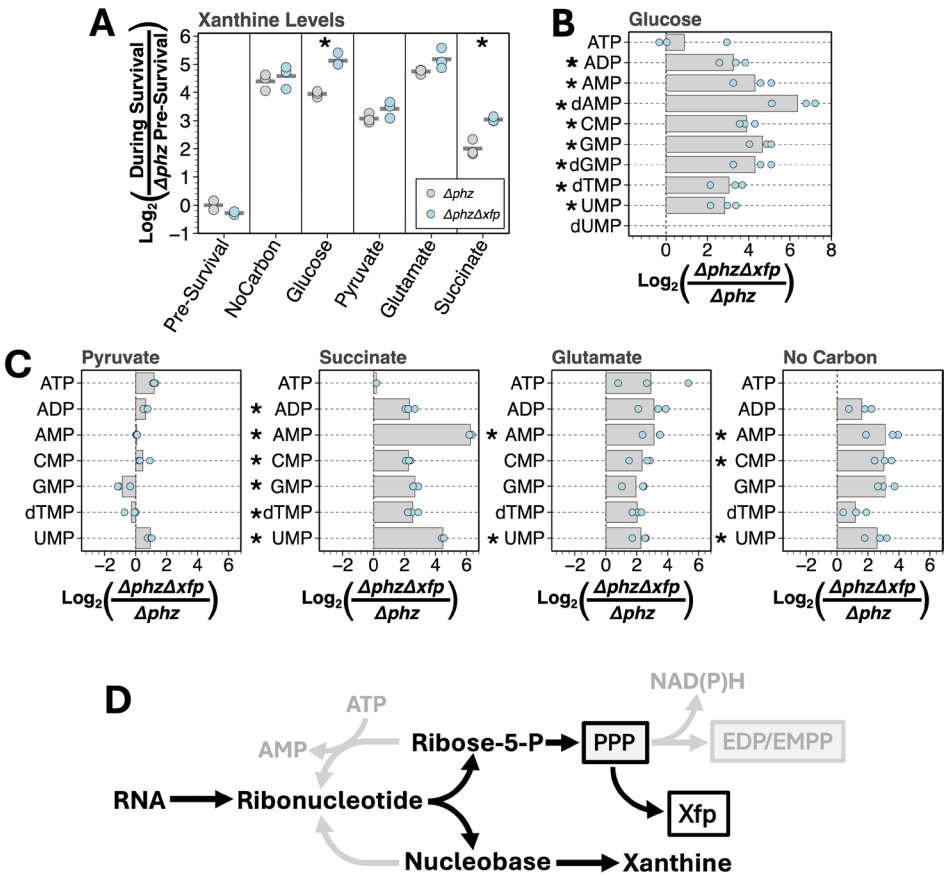


FIGURE 5 | Ribonucleotide salvage occurs during anaerobic survival on all conditions irrespective of *xfp*, but Xfp is important for maintaining ribonucleotide homeostasis under all nutrient conditions except pyruvate. (A) Log_2 transformed xanthine intensities after 3 days of anaerobic survival on various carbon sources, normalized to the mean xanthine level in *Δphz* strain before survival. Grey = *Δphz*, blue = *ΔphzΔxfp*. (B, C) Log_2 transformed *ΔphzΔxfp* metabolite intensities normalized to mean *Δphz* metabolite intensities after 3 days of anaerobic survival on various carbon sources. (A–C) Dashes/bars = mean. Dots = independent replicates, $n = 3$. * denotes p value < 0.05 from an independent two-tailed t-test comparing the means of each strain per metabolite per condition. All carbon sources were at a final concentration for 120 mM of total carbon (e.g., 20 mM glucose, 40 mM pyruvate, etc.) (D) Condensed metabolic diagram of ribonucleotide salvage showing that ribonucleotide degradation produces ribose-5P and nucleobases, the former enters the PPP where it can exit via ATP-costly ribonucleotide biosynthesis, reducing equivalent-generating EDP/EMPP pathways, or via PA14's Xfp. Nucleobases can either be consumed via ribonucleotide biosynthesis or be further degraded to form xanthine. Black arrows represent pathways that would be uninhibited during energy-limited reductive stress survival while grey arrows/pathways are those we believe would be inhibited during anaerobic survival.

ADP, but not ATP levels in the *ΔphzΔxfp* strain compared to *Δphz* cells, suggests that Xfp plays a role in maintaining the cellular energy state as such changes would lead to a lower adenylate charge, which could inhibit functions such as biosynthesis or nutrient transport.

3 | Discussion

Bacteria are commonly found in growth-arrested states; however, the metabolic networks supporting survival under such conditions are understudied even in model organisms such as *P. aeruginosa*. Based on studies performed during active growth, *P. aeruginosa* has been assumed to only catabolize glucose via the EDP (Kohlstedt and Wittmann 2019; Lessie and Phibbs 1984), yet here we show that during anaerobic survival it relies on the PPP and a phosphoketolase-dependent pathway, allowing it to mitigate metabolic dysregulation and death. While phosphoketolases occur across the bacterial tree of life, hitherto, their study has focused almost entirely on their role in fermentative metabolisms in obligate anaerobes or their use in natural product generation and synthetic biology (Årsköld et al. 2008; Bogorad et al. 2013; Bruinsma et al. 2023; de Vries and Stouthamer 1967; Fleige et al. 2011; Krüsemann et al. 2018; Liu et al. 2012; Sánchez et al. 2010). Our contribution to bacterial physiology in this study has been to demonstrate that phosphoketolases can also support viability and ribonucleotide homeostasis during oxidant-limited growth arrest in a historically deemed "non-fermentative" or "obligately aerobic" bacterium. Because cancer cell mitochondria experience reductive stress-induced metabolic disruptions similar to those observed in our system, our findings embody the principle of "unity in biochemistry" first articulated by Albert Kluyver over a century ago (Kluyver 1924).

It is noteworthy that routing of metabolism through the PPP and a phosphoketolase to support anoxic sugar catabolism is shared between fermentative obligate anaerobes, such as Bifidobacterium, Lactobacillus, or Clostridia species, and *P. aeruginosa*, which cannot grow fermentatively (Aristilde

13652958, 2026, 5, Downloaded from https://onlinelibrary.wiley.com/doi/10.1111/mmi.70059 by Claremont Colleges Libraries, Wiley Online Library on [17/11/2026]. See the Terms and Conditions (https://onlinelibrary.wiley.com/terms-and-conditions) on Wiley Online Library for rules of use; OA articles are governed by the applicable Creative Commons License

et al. 2015; Årsköld et al. 2008; de Vries and Stouthamer 1967; Liu et al. 2012; Sánchez et al. 2010). It reinforces the view that the conceptual divide between "fermenters" and "non-fermenters", or "obligate aerobes" as *P. aeruginosa* is commonly but erroneously called, requires reconsideration. Further research investigating whether Xfp-products can be used as electron acceptors would clarify whether *P. aeruginosa* is capable of Xfp-mediated fermentation decoupled from growth. Moreover, we show *P. aeruginosa* carries out significant purine degradation during anaerobic survival and reveal an additional role for phosphoketolases in maintaining ribonucleotide homeostasis within this context. Ribonucleotide recycling is a metabolic necessity for various bacteria during growth arrest, especially during nutrient starvation (Condon 2007; Deutscher 2003; Himeoka et al. 2022); yet whether phosphoketolases facilitate this process in other bacteria during growth arrest remains to be determined. However, the importance of phosphoketolases to support PPP flux and therefore generation of ribonucleotide precursors in various species during fermentative of sugars supports the feasibility of such a role (Aristilde et al. 2015; Aristilde 2017; Årsköld et al. 2008; de Vries and Stouthamer 1967; Sánchez et al. 2010). Regardless, as research into the biology of growth arrest increases, particularly as induced by oxidant limitation, our ability to identify metabolic strategies that transcend historical growth-oriented classifications and taxonomic distance will improve.

In this vein, we speculate that organisms such as *P. aeruginosa* may have evolved to survive but not grow under reductive stress. *P. aeruginosa* prefers non-fermentative easily respirable carbon sources (such as organic acids as opposed to sugars), lacks a few key fermentative genes while containing others, and is unable to use the major NADPH-producing oxidative PPP (Eschbach et al. 2004; Lessie and Phibbs 1984; McGill et al. 2021). Meanwhile, it also produces phenazines (diffusible electron shuttles) that support non-growth maintenance metabolisms in the absence of terminal electron acceptors (Ciemniecki et al. 2024; Glasser et al. 2014). Our discovery that a phosphoketolase supports anaerobic survival, but not growth, furthers this speculation and demonstrates the multitude of complementary strategies this bacterium uses to survive oxidant limitation. Such a strategy might act to bolster stress tolerance under such conditions while conserving resources for use upon reintroduction of a terminal electron acceptor.

Under energy limited anaerobic survival conditions, the upper EMPP and PPP may represent a metabolite "reservoir" with Xfp acting as a release valve. The non-oxidative PPP represents the only cyclable central carbon metabolic network in PA14 that produces no reducing equivalents or requires ATP expenditure. Yet, all exits from the PPP (except by way of Xfp) quickly generate reducing equivalents—lower EMPP—or require ATP expenditure—biosynthesis (Figure 5D) (Kohlstedt and Wittmann 2019). Extensive use of such cycling is supported by the presence of doubly or triply labelled PPP and upper EMPP metabolites in *Δphz* cells during anaerobic survival on glucose (Figure 3B, Figure S3B). Therefore, while Xfp can stimulate energy conservation via substrate phosphorylation during acetate production, we suggest that Xfp's primary role is to maintain metabolic homeostasis via consumption of accumulated metabolites in the PPP. This conclusion is supported by the lower survival of *Δxfp* strains on glucose compared to strains lacking only *ΔackAΔpta*. However, further quantitative flux analysis is required to test this hypothesis. Previous studies in the obligate anaerobe *C. acetobutylicum* have suggested that phosphoketolase-mediated catabolism of pentoses is faster and requires fewer enzymatic steps than catabolism via other PPP enzymes such as transaldolase (Aristilde et al. 2015; Liu et al. 2012). Therefore, it is plausible that during energy-limited anaerobic survival in *P. aeruginosa* such a phosphoketolase-based metabolism may act as an enzymatically "cheaper" and faster way to consume PPP metabolites than other pathways.

The dispensability of Xfp during survival on pyruvate but not on other substrates can also be rationalized (Figure 4A). Pyruvate fermentation does not generate reductive stress because it is redox-balanced (Eschbach et al. 2004; Glasser et al. 2014); it also generates a relatively high adenylate charge ratio and its products (acetate and lactate) can be effluxed to prevent accumulation. Together, these features would enable the cell to maintain balanced PPP metabolism via non-Xfp-mediated pathways (Figure 5D). In contrast, we observed a substantial portion of PPP flux and metabolite accumulation from endogenous carbon stores, one potential source being ribonucleotides. This build-up appears inherent to anaerobic survival, independent of whether Xfp is present, yet Xfp serves to prevent further accumulation and lethality. The survival patterns seen for the parent and *xfp* mutant in the presence of different carbon sources indicate that during anaerobic survival, carbon metabolism acts as a double-edged sword, with increased catabolic flux fueling energy conservation and production of biosynthetic precursors, but at the cost of increased reductive stress, leading to increased pressure on the PPP and metabolite accumulation.

A case in point that illustrates this phenomenon is the importance of balanced ribonucleotide recycling, for which the PPP is vital (Condon 2007; Deutscher 2003; Himeoka et al. 2022). The PPP produces ribose-5P for ribonucleotide biosynthesis and accepts ribose-5P during ribonucleotide degradation (Figure 5D). During anaerobic survival in *P. aeruginosa*, purine degradation occurs in an Xfp-independent manner, evidenced by significant increases to xanthine levels (up to ~64 times higher) across strains and conditions, yet we hypothesize that Xfp ensures the cell's ability to maintain ribonucleotide homeostasis. In fluctuating environments, cells remodel their transcriptome and ribose-5P is generated as a consequence of RNA degradation (Guo and Gross 2014). Because the rate of ribonucleotide degradation during energy-limited growth-arrest likely outpaces the rate of energetically costly ribonucleotide biosynthesis, ribose-5P accumulation would require Xfp to prevent inhibition of ribonucleotide recycling or other catabolic/anabolic flux through the PPP. Catabolism of carbon sources such as glucose during anaerobic survival would then emphasize this role by causing additional PPP metabolite accumulation on top of accumulation via ribonucleotide degradation. This capability of Xfp to regulate these pathways is supported by the absence of PPP metabolite accumulation despite increases to xanthine and ribonucleotide levels in *Δphz* cells during anaerobic survival on glucose. While further work is required to determine Xfp's substrate(s), its homology to a preferentially xylulose-5P degrading phosphoketolase

13652958, 2026, 5, Downloaded from https://onlinelibrary.wiley.com/doi/10.1111/mmi.70059 by Claremont Colleges Libraries, Wiley Online Library on [17/11/2026]. See the Terms and Conditions (https://onlinelibrary.wiley.com/terms-and-conditions) on Wiley Online Library for rules of use; OA articles are governed by the applicable Creative Commons License

(Petrareanu et al. 2014), and its role in modulating ribonucleotide levels suggests that xylulose-5P may be a primary substrate in this organism (Figure S1).

In this vein, an intriguing hypothesis is that Xfp's consumption of ribose-5P, via its equilibration with xylulose-5P, could support redox balance via NAD^+ consumption. Degradation of NAD+ and NADP+, releasing AMP and ribose-5P, may represent a strategy to gain increased control over the cellular redox state (Gazzaniga et al. 2009; Gossmann et al. 2012). Lower levels and/or lack of detection of NADH, NADPH, glutathione, and glutathione disulfide in cells surviving on glucose compared to pyruvate may hint at degradation of redox pools as a general cellular strategy to combat reductive stress. However, the pathways to accomplish such degradation are poorly understood in *P. aeruginosa*.

Alternatively, regulation of PPP metabolite levels by Xfp could avoid energetically costly futile cycling and biosynthesis. During reductive stress and hypoxia, cancer cells have been shown to increase PPP flux and dramatically accumulate ribonucleotides (Wu et al. 2024; Yang et al. 2025). In one study, the authors suggest that reductive stress deregulates ribonucleotide biosynthesis, leading to *de novo* purine biosynthesis and ATP consumption (Yang et al. 2025). Meanwhile, a separate study found that reductive stress led to ribonucleotide accumulation via the far less costly purine salvage pathway, with the resulting increase in ribonucleotide monophosphates inhibiting *de novo* biosynthesis and preventing further energy expenditure (Wu et al. 2024). Additionally, recent work in the cyanobacterium *Synechococcus elongatus* found an Xfp homolog supports survival during light–dark transitions by consuming Calvin-Benson-Bassham cycle metabolites to prevent ATP-consuming futile cycling, albeit at the cost of lower carbon fixation (Lu et al. 2023). In tandem with previous studies in *C. acetobutylicum* suggesting phosphoketolases can act as metabolic "shortcuts" to limit enzymatic costs while hastening pentose catabolism, we speculate that PA14's Xfp consumption of PPP metabolites could avoid futile and energetically costly biosynthesis (Aristilde et al. 2015; Liu et al. 2012; Lu et al. 2023; Servinsky et al. 2012). Such a function could explain why loss of *xfp* is lethal, with buildup of PPP metabolites forcing biosynthesis, draining ATP and disrupting the adenylate charge. Further testing will determine whether this is in fact the case for PA14 and possibly other bacteria.

In summary, our discovery that Xfp facilitates the maintenance of metabolic homeostasis during anaerobic survival under reductive stress reminds us of the adage that "an ounce of prevention is worth a pound of cure". Though we have highlighted Xfp's role in facilitating ribonucleotide homeostasis in *P. aeruginosa* PA14, given that the PPP and acetyl-P derived compounds are integral to many other anabolic processes, it is possible that Xfp could also play a role in amino acid or fatty acid metabolisms, processes known to support bacterial survival during growth arrest (Bergkessel et al. 2016). Additionally, generation of acetyl-P by Xfp may serve as a vital signaling molecule. The parallels seen in the mitochondria literature, where reductively stressed mitochondria are reported to increase ribonucleotide salvage, amino acid biosynthesis, and lipogenesis (Wu et al. 2024; Yang et al. 2025), serve as a powerful reminder of the potential to identify overarching principles of metabolism that span the domains of life as we open our studies of metabolites to include the biology of growth arrest.

4 | Experimental Procedures

4.1 | Strains, Culture Conditions, and Reagents

All strains used can be found in the Table S1. All strains were derived from *P. aeruginosa* UCBPP-PA14 (DKN263, laboratory strain). The *Δphz* strain lacks the *phzA1-G1*, *phzA2-G2* operons, as well as *phzH*, *phzS*, and *phzM* genes (Meirelles et al. 2021). Cells were streaked from 20% glycerol −80°C freezer stocks onto Difco LB 1.5% agar plates (BD Biosciences) and grown overnight at 37°C. *ΔphzΔackAΔpta* strain lacked the *phzA1-G1* and *phzA2-G2* operons as well as the *ackA* and *pta* genes (Glasser et al. 2014). The *ΔphzΔxfp* (this study) strain lacked all genes of the *Δphz* strain including *PA14_17580* encoding a putative phosphoketolase. The *ΔphzΔackAΔptaΔxfp* (this study) gene lacked all genes of the *ΔphzΔackAΔpta* strain including *PA14_17580*.

4.2 | Mutant Generation and Complementation

All plasmids and primers used can be found in the Table S1. Primers were ordered from Integrated DNA technologies. For mutant generation we utilized allelic exchange. Plasmids were synthesized using Gibson assembly (NEB) (Gibson et al. 2009). The plasmid pMQ30 (Shanks et al. 2006) was digested with SmaI, 1 kb regions flanking *PA14_17580* were inserted, and the plasmid was transformed into *E. coli* S17 and conjugated into *P. aeruginosa* PA14. PA14 conjugates were selected on LB + 70 μg/mL gentamicin and 20 μg/mL of chloramphenicol. Final mutants were then selected on LB + 10% sucrose and no NaCl. Complementation was done by addition of *PA14_17580* to the multicloning site of pJM220 (Choi and Schweizer 2006) under control of a L-rhamnose inducible promoter and transformed into *E. coli* S17. *PA14_17580* was then inserted in trans at the attTn7 site of PA14.

4.3 | Balch Tube Anaerobic Survival Assays and Viability Measurements

Planktonic cultures were made with 7 mL of Difco LB and grown for 20 h at 37°C at 250 RPM to reach late stationary phase, OD_{500nm} ~5. A MOPS minimal media (MM) was used for all experiments (100 mM anhydrous MOPS, 9.3 mM NH_4Cl, 3.7 mM KH_2PO_4, 1 mM $MgSO_4$, 30 μM $FeSO_4$ dissolved in EDTA, and 1× HAquil trace metals mix lacking $FeCl_3$) (Martocello et al. 2019). Cell suspensions for all experiments were prepared by washing stationary phase cells 3× at 10,000×g for 10 min at 4°C with resuspension in MOPS MM, then resuspended to a final volume of 200 μL, the OD_{500nm} measured, and the suspension diluted to an OD_{500nm} of ~75. Cell suspensions were then transferred to an anaerobic Coy Chamber with an atmosphere of N_2 and ~1.5%–2.5% H_2. Cell suspensions were diluted 5× with N_2 sparged MOPS MM. N_2 sparged MOPS MM, 250 μL of N_2 sparged carbon sources, and 250 μL of cell suspensions were added to Balch tubes to reach

13652958, 2026, 5, Downloaded from https://onlinelibrary.wiley.com/doi/10.1111/mmi.70059 by Claremont Colleges Libraries, Wiley Online Library on [17/11/2026]. See the Terms and Conditions (https://onlinelibrary.wiley.com/terms-and-conditions) on Wiley Online Library for rules of use; OA articles are governed by the applicable Creative Commons License

a final concentration of $OD_{500nm} = 0.75$ of cells and 120 mM carbon atoms (e.g., 20 mM glucose or 40 mM pyruvate) in a final volume of 5 mL. Balch tubes were then stoppered and crimped before being removed from the Coy Chamber and left to incubate at 30°C at 250 RPM. All Balch tubes, pipettes, and stoppers used were left to passively degas for 5+ days before their use above. Sparging occurred for 30+ min in all steps.

To measure CFU/mL of anaerobically surviving cells in Balch tubes, 1 mL syringes with a INSERT GAUGE needle were fully filled and emptied 5 times under a steady flow of N_2 to remove oxygen, then inserted into Balch tubes and ~200 μL withdrawn and placed in a 96 well plate (Fischer). To confirm no large inputs of oxygen during this, a Balch tube prepared above was given resazurin which is reduced to colorless by cells and reoxidized by oxygen, turning a bright pink. No pink was seen when inserting or withdrawing media for CFU sampling. Samples were serially-diluted at 10× dilution steps, then 5 μL was platted onto Difco LB + 1.5% agar plates and left to incubate overnight at 37°C before CFUs were counted.

4.4 | 96-Well Potentiostat Anaerobic Survival Assays

Cell suspensions were prepared as in Balch tube experiments, but added to a 96-well electrochemical plate at a final cell OD_{500nm} of 0.75, with 20 mM glucose, set concentrations of phenazine-1-carboxamide (PCN), and MOPS MM to a final volume of 200 μL. PCN was solubilized in DMSO. Samples given 0 μM PCN were given an equal volume of DMSO as a vehicle control. Plates were sealed using both a slit-seal cover (BioChromato #R80.120.00) and an aluminum seal cover (DiversifiedBiotech #ALUM-1000). Each well contained a screen-printed carbon working electrode and counter electrode, and Ag/AgCl reference electrode. The plate was incubated at 33°C without shaking in a custom 96-potentiostat system developed at the National Institute for Materials Science, Japan. Every well's working electrode was held at a constant 0 mV vs. Ag/AgCl. On set days, the aluminum seal was removed and wells mixed by pipetting 150 uL several times. 10 μL was removed and transferred to a 96 well plate and CFUs measured as described above for Balch tube experiments.

4.5 | Metabolite Extractions

On select days of anaerobic survival in Balch tubes, the full 7 mL cell suspension ($OD_{600} = 0.75$) was collected by vacuum filtration onto Whatman 0.22 μm nylon filters. Flow-through was collected and frozen at −80°C for downstream measurement of acetate. For collection of intracellular metabolites, filters were dunked upside down in 2 mL cold quenching solution of 40/40/20 methanol/acetonitrile/water (v/v) and incubated at −20°C for 30 min. Quenching solution was pipetted up and down over the filter to remove cell debris and the cell suspension was transferred into 2-mL tubes followed by centrifugation at 10,000 *g* at 4°C for 5 min. The supernatant (200 μL) was aliquoted and dried on ice under flow of N_2. Dried samples were stored at −80°C until analysis.

4.6 | Intracellular Metabolite Quantification

Intracellular metabolites were quantified based on an established metabolomics protocol using UHPLC (Thermo Fisher Scientific Dionex UltiMate 3000) coupled to high-resolution mass spectrometry (Thermo Fisher Scientific Q Exactive quadrupole-Orbitrap) operating in negative mode (Aristilde et al. 2017). For LC we used an Acquity UPLC BEH C18 Column (particle size 1.7 μm, 2.1 mm × 100 mm) maintained at 25°C with an injection volume of 10 μL. The eluents consisted of 97:3 (v/v) water: methanol with 15 mM acetic acid and 10 mM tributylamine (eluent A) and methanol (eluent B) (Aristilde et al. 2017). The flow rate was 0.18 mL min^{-1} (Aristilde et al. 2017). Relative intensities and the fraction of ^{13}C isotopologues of each metabolite was analyzed using the Metabolomic Analysis and Visualization Engine (MAVEN) software (2011.6.17) (Clasquin et al. 2012). IsoCor v2.2.0 was used to correct for natural abundance of ^{13}C (Millard et al. 2019).

4.7 | Determination of ^{13}C Incorporation Into Acetate

Extracellular supernatant samples were thawed and diluted 20:1 (sample: acid) with 1 M H_2SO_4. Low pH assured efficient transfer of acetate as acetic acid in the gas phase processes involved in GC-MS analysis. Samples were analyzed with an Agilent 6890 gas chromatograph coupled to a Waters GCT Premier time-of-flight mass spectrometer operating in electron impact positive ion mode. Samples (500 nL) were injected via a split/splitless injector operated in split mode (20:1) at 250°C. A Phenomenex Focusliner (single taper with wool) (p/n AG0-4680) was installed in the injector. The instrument was tuned to 6000 resolution (m/Δm) and continuous accurate mass calibration was maintained by locking the mass axis to the $C_4F_9^+$ (218.98508 m/z) ion obtained by continuous admission of perfluorotributylamine via the reference reservoir. Spectra were recorded from 33 to 400 m/z beginning at 2.3 min until 10 min. Separation of acetate from other components of the sample was achieved on a ZB-FFAP column (Phenomenex, Torrance, CA) 30 m × 0.32 mm ID × 0.25 μm operated at a constant flow of 0.8 mL/min. Initial column temperature was 100°C for 2 min increasing to 124°C at 8°C/min, then increasing to 180°C at 25°C with a final hold for 3 min. Acetic acid was eluted at 6.9 min. Masslynx and QuanLynx (Version 4.1) software was employed for data processing using peak areas of 60, 61, and 62 m/z for unlabelled, singly ^{13}C-labelled, and doubly ^{13}C-labelled acetic acid, respectively. HCO2+ ions resulting from in-source fragmentation of acetic acid were used to determine labeling at the carboxylate carbon based on the areas of the peaks 45 and 46 m/z for un-labelled and singly ^{13}C labelled fragments, respectively. Ratios of peak areas of labelled to unlabeled ions were used to estimate relative amounts of ^{13}C labelling without further correction.

4.8 | Statistical Analysis and Data Visualization

Unpaired two-tailed *t*-test was applied to determine difference of means between two groups while on-qay analysis of variance

13652958, 2026, 5, Downloaded from https://onlinelibrary.wiley.com/doi/10.1111/mmi.70059 by Claremont Colleges Libraries, Wiley Online Library on [17/11/2026]. See the Terms and Conditions (https://onlinelibrary.wiley.com/terms-and-conditions) on Wiley Online Library for rules of use; OA articles are governed by the applicable Creative Commons License

(ANOVA) was employed to evaluate difference of means between more than two conditions. Tukey's honestly significant difference test was used for pairwise comparisons following a significant ANOVA result. p Value threshold for all tests set at 0.05. All data was analyzed and processed in a Python (3.13.2) using Pandas (2.2.3), NumPy (2.1.3), SciPy (1.15.2), and Statsmodels (0.14.4). All plotting was done using Bokeh (2.2.3). Homology between the phosphoketolase amino acid sequences of *P. aeruginosa* UCBPP-PA14 and *P. aeruginosa* ATCC 15442 was done using Benchling (https://benchling.com).

Author Contributions

Richard D. Horak: conceptualization, methodology, validation, formal analysis, investigation, data curation, visualization, writing – original draft preparation, and writing – review and editing. Nanqing Zhou: conceptualization, methodology, validation, formal analysis, data curation, and writing – review and editing. Korbinian O. Thalhammer: methodology, validation, and writing – review and editing. Nathan F. Dalleska: methodology, validation, and writing – review and editing. Ludmilla Aristilde: conceptualization, methodology, writing – review and editing, and project administration. Dianne K. Newman: conceptualization, writing – review and editing, supervision, project administration, and funding acquisition.

Acknowledgments

We would like to thank the various Newman lab members for their advice throughout the project. We thank Dr. Xiayou Shan (Caltech—Newman Lab) for assistance in initial hypothesis generation and Dr. Scott Saunders (UT Southwestern) for the preliminary tn-seq screen used to generate our hypothesis. This work was supported by grants from the NIH (2R01AI127850-06A1).

Funding

This work was supported by the National Institutes of Health (2R01AI127850-06A1).

Ethics Statement

The authors have nothing to report.

Conflicts of Interest

The authors declare no conflicts of interest.

Data Availability Statement

Metabolomics MS data are freely available through the MetaboLights depository (https://www.ebi.ac.uk/metabolights/) under accession (MTBLS13293). Data and code used in the generation of all figures can be found in the Appendix S1.

References

Aristilde, L. 2017. "Metabolite Labelling Reveals Hierarchies in *Clostridium acetobutylicum* That Selectively Channel Carbons From Sugar Mixtures Towards Biofuel Precursors." *Microbial Biotechnology* 10, no. 1: 162–174. https://doi.org/10.1111/1751-7915.12459.

Aristilde, L., I. A. Lewis, J. O. Park, and J. D. Rabinowitz. 2015. "Hierarchy in Pentose Sugar Metabolism in *Clostridium acetobutylicum*." *Applied and Environmental Microbiology* 81, no. 4: 1452–1462. https://doi.org/10.1128/AEM.03199-14.

Aristilde, L., M. L. Reed, R. A. Wilkes, et al. 2017. "Glyphosate-Induced Specific and Widespread Perturbations in the Metabolome of Soil Pseudomonas Species." *Frontiers in Environmental Science* 5: 266266. https://doi.org/10.3389/fenvs.2017.00034.

Årsköld, E., E. Lohmeier-Vogel, R. Cao, S. Roos, P. Rådström, and E. W. J. van Niel. 2008. "Phosphoketolase Pathway Dominates in Lactobacillus Reuteri ATCC 55730 Containing Dual Pathways for Glycolysis." *Journal of Bacteriology* 190, no. 1: 206–212. https://doi.org/10.1128/jb.01227-07.

Baier, F., and N. Tokuriki. 2014. "Connectivity Between Catalytic Landscapes of the Metallo-β-Lactamase Superfamily." *Journal of Molecular Biology* 426, no. 13: 2442–2456. https://doi.org/10.1016/j.jmb.2014.04.013.

Bartacek, J., J. Zabranska, and P. N. L. Lens. 2007. "Developments and Constraints in Fermentative Hydrogen Production." *Biofuels, Bioproducts & Biorefining* 1, no. 3: 201–214. https://doi.org/10.1002/bbb.17.

Bergkessel, M., D. W. Basta, and D. K. Newman. 2016. "The Physiology of Growth Arrest: Uniting Molecular and Environmental Microbiology." *Nature Reviews Microbiology* 14, no. 9: 549–562. https://doi.org/10.1038/nrmicro.2016.107.

Berney, M., C. Greening, R. Conrad, W. R. Jacobs Jr., and G. M. Cook. 2014. "An Obligately Aerobic Soil Bacterium Activates Fermentative Hydrogen Production to Survive Reductive Stress During Hypoxia." *Proceedings of the National Academy of Sciences* 111, no. 31: 11479–11484. https://doi.org/10.1073/pnas.1407034111.

Bogorad, I. W., T.-S. Lin, and J. C. Liao. 2013. "Synthetic Non-Oxidative Glycolysis Enables Complete Carbon Conservation." *Nature* 502, no. 7473: 693–697. https://doi.org/10.1038/nature12575.

Bruinsma, L., M. Martin-Pascual, K. Kurnia, et al. 2023. "Increasing Cellular Fitness and Product Yields in *Pseudomonas putida* Through an Engineered Phosphoketolase Shunt." *Microbial Cell Factories* 22, no. 1: 14. https://doi.org/10.1186/s12934-022-02015-9.

Cantó, C., K. J. Menzies, and J. Auwerx. 2015. "NAD+ Metabolism and the Control of Energy Homeostasis: A Balancing Act Between Mitochondria and the Nucleus." *Cell Metabolism* 22, no. 1: 31–53. https://doi.org/10.1016/j.cmet.2015.05.023.

Choi, K.-H., and H. P. Schweizer. 2006. "Mini-Tn7 Insertion in Bacteria With Single attTn7 Sites: Example *Pseudomonas aeruginosa*." *Nature Protocols* 1, no. 1: 153–161. https://doi.org/10.1038/nprot.2006.24.

Chubukov, V., L. Gerosa, K. Kochanowski, and U. Sauer. 2014. "Coordination of Microbial Metabolism." *Nature Reviews Microbiology* 12, no. 5: 327–340. https://doi.org/10.1038/nrmicro3238.

Ciemniecki, J. A., C. L. Ho, R. D. Horak, A. Okamoto, and D. K. Newman. 2024. "Mechanistic Study of a Low-Power Bacterial Maintenance State Using High-Throughput Electrochemistry." *Cell* 187, no. 24: 6882–6895. https://doi.org/10.1016/j.cell.2024.09.042.

Ciemniecki, J. A., and D. K. Newman. 2020. "The Potential for Redox-Active Metabolites to Enhance or Unlock Anaerobic Survival Metabolisms in Aerobes." *Journal of Bacteriology* 202, no. 11: 10–128. https://doi.org/10.1128/jb.00797-19.

Clasquin, M. F., E. Melamud, and J. D. Rabinowitz. 2012. "LC-MS Data Processing With MAVEN: A Metabolomic Analysis and Visualization Engine." *Current Protocols in Bioinformatics* 37, no. 1: 14.11.1–14.11.23. https://doi.org/10.1002/0471250953.bi1411s37.

Condon, C. 2007. "Maturation and Degradation of RNA in Bacteria." *Current Opinion in Microbiology* 10, no. 3: 271–278. https://doi.org/10.1016/j.mib.2007.05.008.

Cowley, E. S., S. H. Kopf, A. LaRiviere, W. Ziebis, and D. K. Newman. 2015. "Pediatric Cystic Fibrosis Sputum Can be Chemically Dynamic, Anoxic, and Extremely Reduced due to Hydrogen Sulfide Formation." *MBio* 6, no. 4: 10–1128. https://doi.org/10.1128/mbio.00767-15.

13652958, 2026, 5, Downloaded from https://onlinelibrary.wiley.com/doi/10.1111/mmi.70059 by Claremont Colleges Libraries, Wiley Online Library on [17/11/2026]. See the Terms and Conditions (https://onlinelibrary.wiley.com/terms-and-conditions) on Wiley Online Library for rules of use; OA articles are governed by the applicable Creative Commons License

de Vries, W., and A. H. Stouthamer. 1967. "Pathway of Glucose Fermentation in Relation to the Taxonomy of Bifidobacteria." *Journal of Bacteriology* 93, no. 2: 574–576. https://doi.org/10.1128/jb.93.2.574-576.1967.

Deutscher, M. P. 2003. "Degradation of Stable RNA in Bacteria." *Journal of Biological Chemistry* 278, no. 46: 45041–45044. https://doi.org/10.1074/jbc.R300031200.

Dzurová, L., F. Forneris, S. Savino, P. Galuszka, J. Vrabka, and I. Frébort. 2015. "The Three-Dimensional Structure of 'Lonely Guy' From Claviceps Purpurea Provides Insights Into the Phosphoribohydrolase Function of Rossmann Fold-Containing Lysine Decarboxylase-Like Proteins." *Proteins: Structure, Function, and Bioinformatics* 83, no. 8: 1539–1546. https://doi.org/10.1002/prot.24835.

Enfors, S.-O., M. Jahic, A. Rozkov, et al. 2001. "Physiological Responses to Mixing in Large Scale Bioreactors." *Journal of Biotechnology* 85, no. 2: 175–185. https://doi.org/10.1016/S0168-1656(00)00365-5.

Eschbach, M., K. Schreiber, K. Trunk, J. Buer, D. Jahn, and M. Schobert. 2004. "Long-Term Anaerobic Survival of the Opportunistic Pathogen *Pseudomonas aeruginosa* via Pyruvate Fermentation." *Journal of Bacteriology* 186, no. 14: 4596–4604. https://doi.org/10.1128/jb.186.14.4596-4604.2004.

Ferrara, S., R. Carrubba, S. Santoro, and G. Bertoni. 2021. "The Small RNA ErsA Impacts the Anaerobic Metabolism of *Pseudomonas aeruginosa* Through Post-Transcriptional Modulation of the Master Regulator Anr." *Frontiers in Microbiology* 12: 691608. https://doi.org/10.3389/fmicb.2021.691608.

Fleige, C., J. Kroll, and A. Steinbüchel. 2011. "Establishment of an Alternative Phosphoketolase-Dependent Pathway for Fructose Catabolism in *Ralstonia eutropha* H16." *Applied Microbiology and Biotechnology* 91, no. 3: 769–776. https://doi.org/10.1007/s00253-011-3284-5.

Gayon, U., and G. A. Dupetit. 1886. "Recherches sur la réduction des nitrates par les infiniment petits/par MM. *U. Gayon et G. Dupetit; Station agronomique de Bordeaux*." 1845–1929. https://gallica.bnf.fr/ark:/12148/bpt6k9366473.

Gazzaniga, F., R. Stebbins, S. Z. Chang, M. A. McPeek, and C. Brenner. 2009. "Microbial NAD Metabolism: Lessons From Comparative Genomics." *Microbiology and Molecular Biology Reviews* 73, no. 3: 529–541. https://doi.org/10.1128/mmbr.00042-08.

Gibson, D. G., L. Young, R.-Y. Chuang, J. C. Venter, C. A. Hutchison III, and H. O. Smith. 2009. "Enzymatic Assembly of DNA Molecules up to Several Hundred Kilobases." *Nature Methods* 6, no. 5: 343–345. https://doi.org/10.1038/nmeth.1318.

Glasser, N. R., S. E. Kern, and D. K. Newman. 2014. "Phenazine Redox Cycling Enhances Anaerobic Survival in *Pseudomonas aeruginosa* by Facilitating Generation of ATP and a Proton-Motive Force." *Molecular Microbiology* 92, no. 2: 399–412. https://doi.org/10.1111/mmi.12566.

Gossmann, T. I., M. Ziegler, P. Puntervoll, L. F. de Figueiredo, S. Schuster, and I. Heiland. 2012. "NAD+ Biosynthesis and Salvage—A Phylogenetic Perspective." *FEBS Journal* 279, no. 18: 3355–3363. https://doi.org/10.1111/j.1742-4658.2012.08559.x.

Guo, M. S., and C. A. Gross. 2014. "Stress-Induced Remodeling of the Bacterial Proteome." *Current Biology* 24, no. 10: R424–R434. https://doi.org/10.1016/j.cub.2014.03.023.

Hackmann, T. J. 2024. "The Vast Landscape of Carbohydrate Fermentation in Prokaryotes." *FEMS Microbiology Reviews* 48, no. 4: fuae016. https://doi.org/10.1093/femsre/fuae016.

Hackmann, T. J., and B. Zhang. 2023. "The Phenotype and Genotype of Fermentative Prokaryotes." *Science Advances* 9, no. 39: eadg8687. https://doi.org/10.1126/sciadv.adg8687.

Hammond, J. H., E. F. Dolben, T. J. Smith, S. Bhuju, and D. A. Hogan. 2015. "Links Between Anr and Quorum Sensing in *Pseudomonas aeruginosa* Biofilms." *Journal of Bacteriology* 197, no. 17: 2810–2820. https://doi.org/10.1128/jb.00182-15.

Himeoka, Y., B. Gummesson, M. A. Sørensen, S. L. Svenningsen, and N. Mitarai. 2022. "Distinct Survival, Growth Lag, and rRNA Degradation Kinetics During Long-Term Starvation for Carbon or Phosphate." *mSphere* 7, no. 3: e01006–e01021. https://doi.org/10.1128/msphere.01006-21.

Kluyver, A. J. 1924. "Unity and Diversity in the Metabolism of Micro-Organisms." https://lib.guides.umbc.edu/ld.php?content_id=46752710.

Kohlstedt, M., and C. Wittmann. 2019. "GC-MS-Based 13C Metabolic Flux Analysis Resolves the Parallel and Cyclic Glucose Metabolism of *Pseudomonas putida* KT2440 and *Pseudomonas aeruginosa* PAO1." *Metabolic Engineering* 54: 35–53. https://doi.org/10.1016/j.ymben.2019.01.008.

Krüsemann, J. L., S. N. Lindner, M. Dempfle, et al. 2018. "Artificial Pathway Emergence in Central Metabolism From Three Recursive Phosphoketolase Reactions." *FEBS Journal* 285, no. 23: 4367–4377. https://doi.org/10.1111/febs.14682.

Kukurugya, M. A., S. Rosset, and D. V. Titov. 2024. "The Warburg Effect Is the Result of Faster ATP Production by Glycolysis Than Respiration." *Proceedings of the National Academy of Sciences* 121, no. 46: e2409509121. https://doi.org/10.1073/pnas.2409509121.

Lessie, T. G., and P. V. Phibbs. 1984. "Alternative Pathways of Carbohydrate Utilization in Pseudomonads." *Annual Review of Microbiology* 38, no. 1: 359–388. https://doi.org/10.1146/annurev.mi.38.100184.002043.

Liu, L., L. Zhang, W. Tang, et al. 2012. "Phosphoketolase Pathway for Xylose Catabolism in *Clostridium acetobutylicum* Revealed by 13C Metabolic Flux Analysis." *Journal of Bacteriology* 194, no. 19: 5413–5422. https://doi.org/10.1128/jb.00713-12.

Lu, K.-J., C.-W. Chang, C.-H. Wang, et al. 2023. "An ATP-Sensitive Phosphoketolase Regulates Carbon Fixation in Cyanobacteria." *Nature Metabolism* 5, no. 7: 1111–1126. https://doi.org/10.1038/s42255-023-00831-w.

Luo, M., X. Ma, and J. Ye. 2024. "Reductive Stress—A Common Metabolic Feature of Obesity and Cancer." *Acta Pharmaceutica Sinica B* 14, no. 12: 5181–5185. https://doi.org/10.1016/j.apsb.2024.08.034.

Martocello, D. E., F. M. M. Morel, and D. L. McRose. 2019. "H-Aquil: A Chemically Defined Cell Culture Medium for Trace Metal Studies in Vibrios and Other Marine Heterotrophic Bacteria." *Biometals* 32, no. 6: 819–828. https://doi.org/10.1007/s10534-019-00215-2.

McGill, S. L., Y. Yung, K. A. Hunt, M. A. Henson, L. Hanley, and R. P. Carlson. 2021. "*Pseudomonas aeruginosa* Reverse Diauxie Is a Multidimensional, Optimized, Resource Utilization Strategy." *Scientific Reports* 11, no. 1: 1457. https://doi.org/10.1038/s41598-020-80522-8.

Meirelles, L. A., E. K. Perry, M. Bergkessel, and D. K. Newman. 2021. "Bacterial Defenses Against a Natural Antibiotic Promote Collateral Resilience to Clinical Antibiotics." *PLoS Biology* 19, no. 3: e3001093. https://doi.org/10.1371/journal.pbio.3001093.

Millard, P., B. Delépine, M. Guionnet, M. Heuillet, F. Bellvert, and F. Létisse. 2019. "IsoCor: Isotope Correction for High-Resolution MS Labeling Experiments." *Bioinformatics* 35, no. 21: 4484–4487. https://doi.org/10.1093/bioinformatics/btz209.

Petrareanu, G., M. C. Balasu, A. M. Vacaru, et al. 2014. "Phosphoketolases From *Lactococcus lactis*, Leuconostoc Mesenteroides and *Pseudomonas aeruginosa*: Dissimilar Sequences, Similar Substrates but Distinct Enzymatic Characteristics." *Applied Microbiology and Biotechnology* 98, no. 18: 7855–7867. https://doi.org/10.1007/s00253-014-5723-6.

Sánchez, B., M. Zúñiga, F. González-Candelas, C. de los Reyes-Gavilán, and A. Margolles. 2010. "Bacterial and Eukaryotic Phosphoketolases: Phylogeny, Distribution and Evolution." *Journal of Molecular Microbiology and Biotechnology* 18, no. 1: 37–51. https://doi.org/10.1159/000274310.

13652958, 2026, 5, Downloaded from https://onlinelibrary.wiley.com/doi/10.1111/mmi.70059 by Claremont Colleges Libraries, Wiley Online Library on [17/11/2026]. See the Terms and Conditions (https://onlinelibrary.wiley.com/terms-and-conditions) on Wiley Online Library for rules of use; OA articles are governed by the applicable Creative Commons License

Saunders, S. 2020. "'Phenazine Survival TnSeq.' CaltechDATA." https://data.caltech.edu/records/bdfca-9rp28.

Seo, H., S. Kim, H.-Y. Sagong, et al. 2016. "Structural Basis for Cytokinin Production by LOG From *Corynebacterium glutamicum*." *Scientific Reports* 6, no. 1: 31390. https://doi.org/10.1038/srep31390.

Servinsky, M. D., K. L. Germane, S. Liu, et al. 2012. "Arabinose Is Metabolized via a Phosphoketolase Pathway in *Clostridium acetobutylicum* ATCC 824." *Journal of Industrial Microbiology and Biotechnology* 39, no. 12: 1859–1867. https://doi.org/10.1007/s10295-012-1186-x.

Shanks, R. M. Q., N. C. Caiazza, S. M. Hinsa, C. M. Toutain, and G. A. O'Toole. 2006. "*Saccharomyces cerevisiae*-Based Molecular Tool Kit for Manipulation of Genes From Gram-Negative Bacteria." *Applied and Environmental Microbiology* 72, no. 7: 5027–5036. https://doi.org/10.1128/AEM.00682-06.

Silver, W. L., A. E. Lugo, and M. Keller. 1999. "Soil Oxygen Availability and Biogeochemistry Along Rainfall and Topographic Gradients in Upland Wet Tropical Forest Soils." *Biogeochemistry* 44, no. 3: 301–328. https://doi.org/10.1007/BF00996995.

Suzuki, R., T. Katayama, B. J. Kim, et al. 2010. "Crystal Structures of Phosphoketolase: Thiamine Diphosphate-Dependent Dehydration Mechanism." *Journal of Biological Chemistry* 285, no. 44: 34279–34287. https://doi.org/10.1074/jbc.M110.156281.

Thauer, R. K., K. Jungermann, and K. Decker. 1977. "Energy Conservation in Chemotrophic Anaerobic Bacteria." *Bacteriological Reviews* 41, no. 1: 100–180. https://doi.org/10.1128/br.41.1.100-180.1977.

Tribelli, P. M., A. M. Lujan, A. Pardo, et al. 2019. "Core Regulon of the Global Anaerobic Regulator Anr Targets Central Metabolism Functions in Pseudomonas Species." *Scientific Reports* 9, no. 1: 9065. https://doi.org/10.1038/s41598-019-45541-0.

Vander Wauven, C., A. Piérard, M. Kley-Raymann, and D. Haas. 1984. "*Pseudomonas aeruginosa* Mutants Affected in Anaerobic Growth on Arginine: Evidence for a Four-Gene Cluster Encoding the Arginine Deiminase Pathway." *Journal of Bacteriology* 160, no. 3: 928–934. https://doi.org/10.1128/jb.160.3.928-934.1984.

Voroney, R. P., and R. J. Heck. 2015. "The Soil Habitat." In *Soil Microbiology, Ecology and Biochemistry*, 15–39. Elsevier. https://doi.org/10.1016/B978-0-12-415955-6.00002-5.

Warburg, O. 1925. "The Metabolism of Carcinoma Cells." *Journal of Cancer Research* 9, no. 1: 148–163. https://doi.org/10.1158/jcr.1925.148.

Wu, Z., D. Bezwada, F. Cai, et al. 2024. "Electron Transport Chain Inhibition Increases Cellular Dependence on Purine Transport and Salvage." *Cell Metabolism* 36, no. 7: 1504–1520. https://doi.org/10.1016/j.cmet.2024.05.014.

Xiao, W., and J. Loscalzo. 2020. "Metabolic Responses to Reductive Stress." *Antioxidants & Redox Signaling* 32, no. 18: 1330–1347. https://doi.org/10.1089/ars.2019.7803.

Yang, R., Z. Guo, and B. Li. 2025. "NADH Reductive Stress Drives Metabolic Reprogramming." *Trends in Cell Biology*. https://doi.org/10.1016/j.tcb.2025.07.005.

Yang, R., C. Yang, L. Ma, et al. 2022. "Identification of Purine Biosynthesis as an NADH-Sensing Pathway to Mediate Energy Stress." *Nature Communications* 13, no. 1: 7031. https://doi.org/10.1038/s41467-022-34850-0.

Ying, W. 2008. "NAD+/NADH and NADP+/NADPH in Cellular Functions and Cell Death: Regulation and Biological Consequences." *Antioxidants & Redox Signaling* 10, no. 2: 179–206. https://doi.org/10.1089/ars.2007.1672.

Zumft, W. G. 1997. "Cell Biology and Molecular Basis of Denitrification." *Microbiology and Molecular Biology Reviews* 61, no. 4: 533–616. https://doi.org/10.1128/mmbr.61.4.533-616.1997.

Supporting Information

Additional supporting information can be found online in the Supporting Information section. **Appendix S1:** mmi70059-sup-0001-AppendixS1.zip. **Figures S1–S10:** mmi70059-sup-0002-FiguresS1-S10.docx. **Table S1:** mmi70059-sup-0003-TableS1.xlsx.

13652958, 2026, 5, Downloaded from https://onlinelibrary.wiley.com/doi/10.1111/mmi.70059 by Claremont Colleges Libraries, Wiley Online Library on [17/11/2026]. See the Terms and Conditions (https://onlinelibrary.wiley.com/terms-and-conditions) on Wiley Online Library for rules of use; OA articles are governed by the applicable Creative Commons License